Research Article Vol. 5, No. 10 / October 2018 / Optica 1171

Multiparameter approach to quantum phase estimation with limited visibility

Emanuele Roccia,[1] Valeria Cimini,[1] Marco Sbroscia,[1,*] Ilaria Gianani,[1] Ludovica Ruggiero,[1] Luca Mancino,[1] Marco G. Genoni,[2] Maria Antonietta Ricci,[1] and Marco Barbieri[1,3]

[1]Dipartimento di Scienze, Università degli Studi Roma Tre, Via della Vasca Navale 84, 00146 Rome, Italy
[2]Quantum Technology Lab, Dipartimento di Fisica, Università degli Studi di Milano, 20133 Milan, Italy
[3]Istituto Nazionale di Ottica—CNR, Largo Enrico Fermi 6, 50125 Florence, Italy
*Corresponding author: marco.sbroscia@uniroma3.it

Received 16 April 2018; revised 26 June 2018; accepted 23 July 2018 (Doc. ID 328571); published 24 September 2018

Optical sensors based on quantum light need to work even in the presence of imperfections. Here we discuss how to address the presence of noise by measuring multiple parameters at once: those we seek to monitor and those linked to the imperfections. Our method is applied to the investigation of the optical activity of sugary solutions limited by reduced visibility. These studies introduce multiparameter estimation as a viable approach to allow for robust operation of quantum sensors as they are developed from fundamental research to technology.

OCIS codes: (120.3940) Metrology; (120.5050) Phase measurement; (160.1585) Chiral media.

https://doi.org/10.1364/OPTICA.5.001171

1. INTRODUCTION

The identification of genuine properties of a system, from single molecules to complex composite systems, represents a primary goal for physical and chemical analysis. As metrological requirements become increasingly demanding in terms of performance, understanding the ultimate precision achievable in the estimation of a parameter represents a key issue. In this respect, quantum metrology, aiming at designing protocols to perform optimal measurements, figures as an appealing and intriguing field of research and applications [1,2].

Phase estimation has long represented the heart of quantum metrology [3–5]: in a large number of technological areas, the estimation problem is concerned with determining a single parameter, and this is typically manifested as a phase shift of the quantum state describing the probe. The engineering of such a state then aims at providing the optimal choice for an enhanced sensitivity in the estimation: particular families of states, as squeezed [6–8] or many-body $N00N$ states [4,9–11], are often used to feed interferometers, showing how nonclassicality represents the primary ingredient of the probe states. Nevertheless, an increase in sensitivity balances the robustness of the quantum state: the more informative these resources are, the more fragile and difficult they are to obtain. The promised quantum advantage can be indeed easily spoiled by ungoverned or spurious couplings with the environment, as it has been shown in the case of interferometry [12–17], and subsequently described in more general no-go theorems [18,19].

In order to circumvent these no-go theorems and observe a quantum enhancement also in the context of noisy quantum metrology, several different approaches have been pursued, based on either considering noise with a particular geometry [20,21], time-inhomogeneous dynamics [22–26], quantum control and error correction methods [27–36], or time-continuous monitoring of the environment [37]; in all these metrological schemes, a proper characterization of the noise affecting the system is, however, required. It is not always the case that such characterization can be performed in advance: for instance, in time-varying cases, the noise process itself can change, and it is then important to design strategies that treat the assessment of both unitary parameters, such as phases, and dissipative parameters, including loss or phase diffusion, at an equal pace by demanding a multiparameter approach. Such extended characterization is akin in spirit to channel tomography [8,38,39], aside from the important difference that one allows for a single choice of probes and not for a tomographically complete family. The multiparameter approach has been the subject of intensive research over the last few years, and this has highlighted the emergence of a trade-off in the achievable precision on individual parameters in many practical instances, ranging from simultaneous estimation of multiple phases (or in general unitary parameters) [40–46] to the case of both unitary and noisy parameters [47–51]. On the other hand, working in a multiparameter setting also brings the advantage of making the estimation process more robust against small deviations of the designed probes from the optimal states [49].

Here we present an estimation experiment in which the multiparameter approach is followed to obtain the value of a phase shift and, at the same time, a reliable estimate of the quality of the probe, as measured by the visibility of the interference fringes.

Differently from [17], where phase estimation with not perfectly indistinguishable photons is investigated, the resources are devoted to both estimation tasks. Hence, by estimating both quantities at the same time, it is possible to reduce biases due to an uncertain knowledge of the probe. We apply this method to the investigation of chiral aqueous solutions of fructose investigated by two-photon $N00N$ states. When focusing on mode indistinguishability, the theoretical generalization to higher photon numbers N demonstrates a variation in the scaling associated to the precision on phase and mode distinguishability depending on the working conditions.

2. TWO-PARAMETER ESTIMATION OF PHASE AND VISIBILITY

A common setup in quantum phase estimation uses single-photon pairs produced via a spontaneous parametric downconversion (SPDC) process: in the typical scheme, the two photons are first combined on a beam splitter (BS), so that Hong–Ou–Mandel interference [52] produces in a $N00N$ state with $N = 2$, i.e., a state in a superposition of two photons being present in either mode and none on the other. The monitored element, imparting a phase shift ϕ, is then inserted on one of the modes, with the other left unperturbed. The detection scheme has the two modes recombined on a second BS and photon counters on the outputs. The combination of the nonclassicality of the state and of the optimality of the measurement choice results in oscillations of the photon counting probabilities occurring with a phase 2ϕ, hence, in a superior precision than attainable with classical light of the same average energy. This strategy, although effective, clashes with the non-ideal visibility v of the two-photon interference on the two BSs: a second characteristic parameter to be estimated is then introduced. This sets the modulation depth of the oscillations, and it is necessary to know it to recover the correct value of ϕ. An incorrect assessment of v would determine a bias on the estimation of the phase. The value of v is limited both by the distinguishability of the two photons in spectral and spatial degrees of freedom, but also to dephasing or depolarization mechanisms taking place inside the sample. Therefore, a preliminary calibration performed under conditions which do not reflect those present at the time of phase estimation might weaken the metrological capabilities of the protocol. We have then explored the alternative approach of assessing the values of ϕ and v simultaneously.

Figure 1 shows the experimental apparatus we used to implement the phase estimation. Two photons with mutually orthogonal polarizations, horizontal (H) and vertical (V), are combined on a polarizing beam splitter (PBS). Having very similar spectra, the two photons are highly indistinguishable, and their perfect interference would produce the $N00N$ state in the left- (L) and right-circular (R) polarization modes,

$$\begin{aligned}\hat{a}_H^\dagger \hat{a}_V^\dagger |0\rangle &= \frac{1}{2}((\hat{a}_R^\dagger)^2 - (\hat{a}_L^\dagger)^2)|0\rangle \\ &= \frac{1}{\sqrt{2}}(|2_R, 0_L\rangle - |0_R, 2_L\rangle). \end{aligned} \tag{1}$$

Introducing a phase ϕ on the R mode is equivalent to rotating a linear polarization by an angle $\phi/2$ and modifies the state as

$$|\psi\rangle = \cos\phi \hat{a}_H^\dagger \hat{a}_V^\dagger |0\rangle - \sin\phi \frac{(\hat{a}_H^\dagger)^2 - (\hat{a}_V^\dagger)^2}{2}|0\rangle. \tag{2}$$

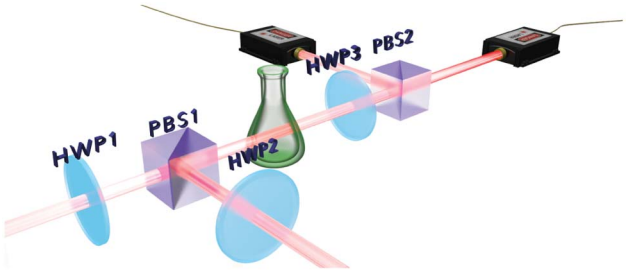

Fig. 1. Experimental setup: each one of the two single photons (wavelength 810 nm) of the pair generated via type-I SPDC from a beta barium borate (BBO, 3 mm length) nonlinear crystal excited via a continuous-wave (80 mW power) pump laser passes through a half-wave plate (HWP1 at 0° and HWP2 at 45°) before being combined on a polarized beam splitter (PBS1). These photons are used to estimate the birefringent phase imparted by the optical activity of a chiral solution. A wave plate (HWP3) and a second polarizer (PBS2) project the outcoming photons onto different polarizations. In the calibration procedure, an additional HWP, not sketched here, replaces the solution to impart a well-defined phase.

The phase ϕ modulates the populations in the states $|\uparrow\rangle = |1_H, 1_V\rangle$ and $|\downarrow\rangle = (|2_H, 0_V\rangle - |0_H, 2_V\rangle)/\sqrt{2}$, which represent the basis of an effective two-level system, i.e., a qubit. The detection scheme consists of a half-wave plate (HWP) and a second PBS, allowing the selection of arbitrary linear polarizations via the angular position θ of the HWP. Photon counting is performed by fiber-coupled avalanche photodiodes (APD) placed on each of the two output arms from the PBS. In the realistic case when the modulations in the state defined in Eq. (2) occur with visibility v, the relevant detection probabilities are

$$\begin{aligned} p(1|\theta;\phi,v) &= \frac{1}{1+v}(1 + v\cos(8\theta - 2\phi)), \\ p(2|\theta;\phi,v) &= \frac{v}{1+v}\sin^2(4\theta - \phi), \end{aligned} \tag{3}$$

where $p(1|\theta;\phi,v)$ describes the probability of a coincidence count between the two arms (associated to $|\uparrow\rangle$), and $p(2|\theta;\phi,v)$ is the probability of finding two photons in one arm (both events are associated to $|\downarrow\rangle$); the proper normalization is $p(1|\theta;\phi,v) + 2p(2|\theta;\phi,v) = 1$. Because of the underlying single-qubit structure of the state in Eq. (2), at least two settings of θ must be chosen to resolve the two parameters; this amounts to performing a positive-operator-valued measurement (POVM) with 2×3 outcomes. Furthermore, since our detectors cannot resolve the photon number, we have actually adopted four settings of θ (viz. $\theta = \{0, \pi/16, \pi/8, 3\pi/16\}$) and used the post-selected probabilities,

$$p(\theta|1;\phi,v) = \frac{1}{4}(1 + v\cos(8\theta - 2\phi)), \tag{4}$$

which only consider the coincidence events for each setting. In the post-selection picture, the probability above treats θ as the outcome of the measurement scheme. Assuming that the four settings are in fact performed randomly, each one with probability 1/4, Eq. (4) quantifies the probability that the coincidence event detected corresponds to the particular setting θ. Data are collected in the form of a vector, $\bar{n}$, formed by four coincidence count rates n_θ, associated to each setting $\theta = \{0, \pi/16, \pi/8, 3\pi/16\}$; therefore, we post-select four out of the possible 4×3 outcomes.

An experimental joint distribution for the measured values of ϕ and v is obtained by Bayesian estimation. This consists in using

Bayes's theorem to update the *a priori* joint probability $P_A(\phi, v)$, based on the knowledge of the measured values n_θ: $P_B(\phi, v|\bar{n}) = \mathcal{N} P_A(\phi, v) \prod_\theta p(\theta|1; \phi, v)^{n_\theta}$ ($\mathcal{N}$ is a normalization constant).

3. EXPERIMENTAL RESULTS

We have tested the performance of our experiment with a calibration step by inserting an additional HWP between the two PBSs; this imparts a set phase φ depending on its angle setting and provides the metrological capabilities of our multiparameter strategy. Figure 2(a) shows, as a function of the imparted phase, the results of the measured of ϕ and v from $P_B(\phi, v|\bar{n})$, quantified as the first moments of the marginal distributions ϕ_B and v_B,

$$\phi_B = \int \phi P_B(\phi, v|\bar{n}) d\phi \mathrm{d}v,$$
$$v_B = \int v P_B(\phi, v|\bar{n}) d\phi \mathrm{d}v, \tag{5}$$

with the integration limits set by the width of $P_A(\phi, v)$. A linear regression of the values highlights the goodness of the phase estimation ϕ, as its slope is $s_\phi = 1.011 \pm 0.004$, in agreement with the expected value 1. Concerning the visibility, the estimation appears to be affected by fluctuations around a constant mean value instead, as the slope of the linear fit of that data confirms, $s_v = -0.001 \pm 0.003$. Such fluctuations are likely to arise from a slight difference in the optical coupling of the initial H photon into each the two detection fibers and similarly for the V photon; this asymmetry comes from free-space operation and can be strongly mitigated by the use of guided optics in actual devices.

A more stringent test in metrology is the verification of the Cramér–Rao bound (CRB). This sets a lower bound to the covariance matrix Σ of the estimated parameters, whose elements are defined as the second moments of $P_B(\phi, v|\bar{n})$,

$$\Delta^2\phi = \Sigma_{\phi,\phi} = \int (\phi - \phi_B)^2 P_B(\phi, v|\bar{n}) d\phi \mathrm{d}v,$$
$$\Delta^2 v = \Sigma_{v,v} = \int (v - v_B)^2 P_B(\phi, v|\bar{n}) d\phi \mathrm{d}v,$$
$$\Sigma_{\phi,v} = \Sigma_{v,\phi} = \int (\phi - \phi_B)(v - v_B) P_B(\phi, v|\bar{n}) d\phi \mathrm{d}v. \tag{6}$$

The measurement strategy is characterized by its Fisher information matrix $\mathcal{F}$, whose elements are

$$\mathcal{F}_{ij} = \sum_\theta \frac{\partial_i p(\theta|\phi, v) \partial_j p(\theta|\phi, v)}{p(\theta|\phi, v)}, \tag{7}$$

with i and j able to correspond to either ϕ or v. The CRB asserts that, given a number of trials M, the covariance matrix is bounded as

$$\Sigma \geq \mathcal{F}^{-1}/M. \tag{8}$$

This matrix inequality holds in the asymptotic limit of a large number of trials and sets lower bounds for the individual

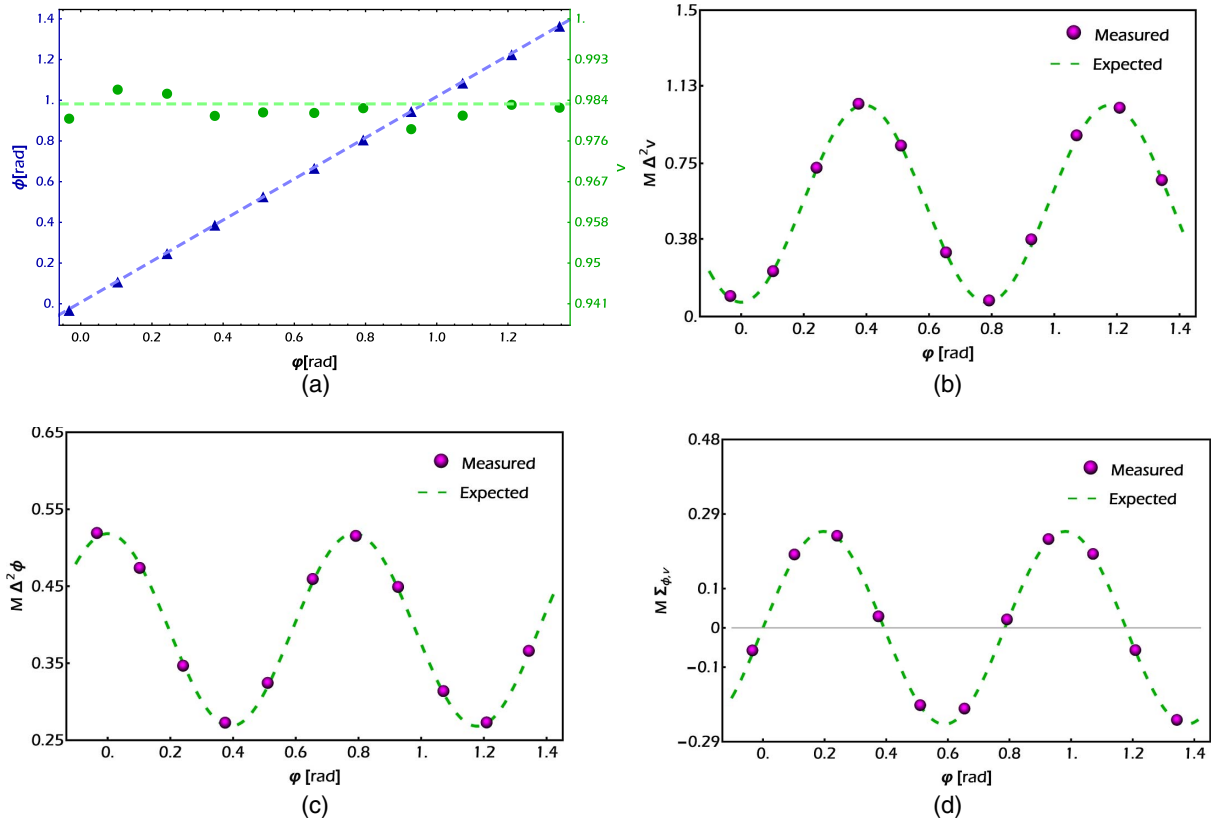

Fig. 2. Multiparameter Bayesian estimation for setup calibration. (a) Estimated phase (blue triangles, left scale) and visibility (green circles; right scale) versus calibration phase, φ, imparted by an HWP. Dashed lines are linear fit of data. (b) and (c) Estimated variance (times the number of resources M) for (b) visibility and (c) phase as a function of the imparted phase. The dashed line represents the corresponding CRBs. (d) Estimated covariance for the visibility and phase as a function of the imparted phase. The dashed line represents the corresponding CRB. All covariance matrices have been estimated from $M \simeq 70$ K repetitions. Error bars are smaller than the marker size for all data.

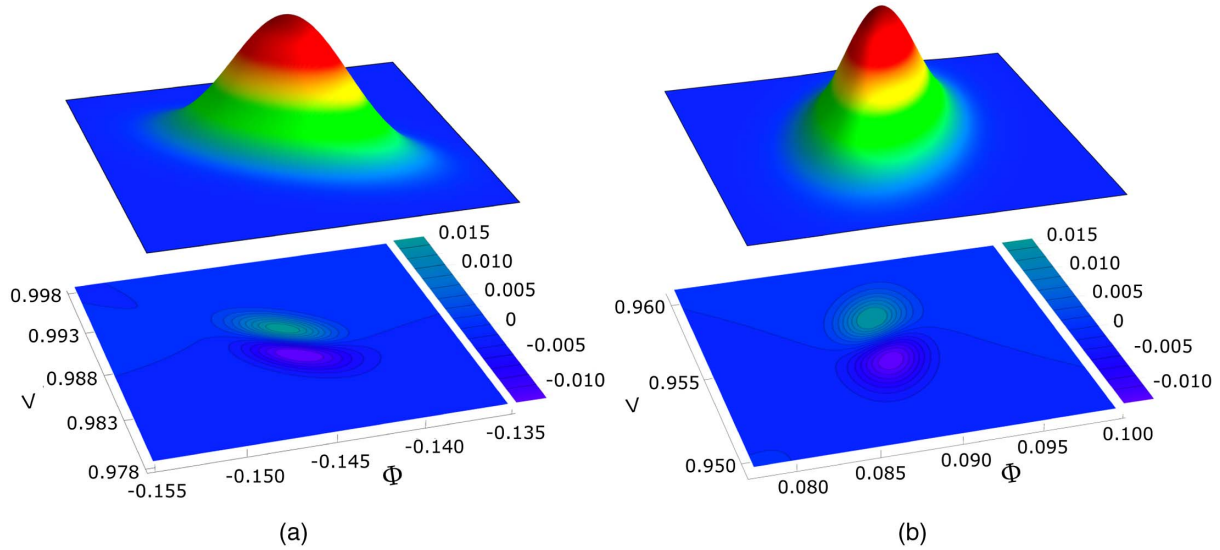

Fig. 3. Upper panels: Bayesian joint probabilities for visibility, V, and phase, Φ; the joint distribution is normalized to unit. Lower panels: difference of the experimental density probability with respect to the one at the CRB for (a) fructose aqueous solution with 0.3 g/ml nominal concentration and (b) sucrose aqueous solution with 0.3 g/ml nominal concentration. A number $M \simeq 50$ K and $M \simeq 75$ K of repetitions have been employed for fructose and sucrose, respectively. The expected probabilities are calculated as a two-dimensional Gaussian with covariance matrix $\mathcal{F}^{-1}/M$; the observed differences between the experiment and the prediction are partly due to deviations from this shape. The V and Φ are the same for the upper and lower panels.

precisions $\Delta^2\phi$ and $\Delta^2 v$, as well as on their covariance $\Sigma_{\phi,v}$. The conditional probabilities in Eq. (7), describing our experiment, correspond to the post-selected coincidence events of our detectors. The effect of post-selection on estimation precision has been described in detail in the literature [53,54], and the consequences on our experimental results are better discussed in Supplement 1. It is important to note that, while post-selection has typically been investigated as a tool to enhance estimation precision, in our case it is a consequence of the limitation of the experimental setup. In Fig. 2 we report the measured uncertainties and covariance in very good agreement to the expected values predicted by the CRB in Eq. (8) with $M = \sum_\theta n_\theta$. Oscillations of the attainable precisions in Eq. (6) can be observed: the available information is distributed between the phase and the visibility, depending on the value of ϕ; covariances are modulated as well, and the best estimation for either individual parameter corresponds to minimal correlation.

As an application of our protocol, we perform the estimation of the phase imparted by aqueous solutions of fructose. It is common knowledge that sugars are an interesting example of chiral molecules, able to impart a rotation to an initial linear polarization. Monitoring their optical activity via light–matter coupling can thus represent a valuable approach to infer information on their interaction with the surroundings. The most relevant environment for their application is the aqueous solution: investigation with quantum light has been undertaken in [55] in a single-parameter approach. Figure 3 reports the Bayesian joint probability distribution for two different sugar aqueous solutions, namely, fructose (F) and sucrose (S), at the same nominal concentration of $c = 0.3$ g/ml. The upper 3D plots show the reconstructed distributions, which give back the following average values $\phi_F = -0.145$ rad and $\phi_S = 0.089$ rad, consistent with the values obtained by using the classical light of a close wavelength (808 nm) in the same apparatus. The underlying contour plots show the difference between the reconstructed distribution and the expected Gaussian saturating the CRB; for both concentrations, the deviations remain of the order of 0.01. In order to assess quantitatively how close our estimation lies to the CRB, we adopt the likelihood ratio test predicting that, under the null hypothesis that Σ saturates Eq. (8), the variable

$$l = M^2 \,\mathrm{Tr}(\mathcal{F}\cdot\Sigma) - M(\ln\ \det(\Sigma) + \ln\ \det(M\mathcal{F})) - 2 \quad (9)$$

is distributed as the χ^2 variable with 3 deg of freedom [56]. The measured values for the two concentrations are $l_F = 2.63$ and $l_S = 0.10$, both compatible with the critical value 7.81 for the 95% confidence interval (see Supplement 1).

4. SCALING LAWS FOR MULTIPARAMETER ESTIMATION

The usefulness of quantum resources is typically assessed by looking at how the precision of given parameters scales with the number of photons N in the probe. For optical phase estimation, quantum probes can reach a scaling law of the Fisher information as N^2, while classical resources are limited to N. For loss, the Fisher information grows with N for both classical and quantum probes [57,58]. For these purposes, we generalized to states with $2N$ photons: we consider Holland–Burnett (HB) states [59] that are obtained by quantum interference of two N photon states arriving on input modes with creation operators $a_H^\dagger$ and $b_V^\dagger$, which are made to interfere. Note that HB states that are equivalent to $N00N$ states for $N = 2$, with each photon entering in one arm of the interferometer, yield the same quantum enhanced scaling $\sim 1/N^2$ in the estimation precision for a generic number of photons; moreover, compared to $N00N$ states, they are more feasible in terms of laboratory resources and have been also shown to be more robust in the presence of loss [15].

As explained in the previous section, a phase ϕ is then inserted, and the detection scheme considers a second interference,

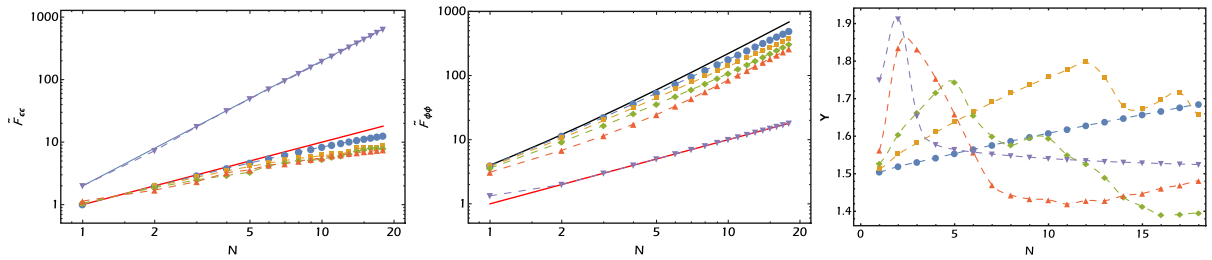

Fig. 4. Scaling of the Fisher information: (a) effective Fisher information for the distinguishability parameter ϵ. The points correspond to numerical results, and the solid lines correspond to $2N^2$ (blue) and N (red). (b) Effective Fisher information for the phase ϕ. The points correspond to numerical results, and the solid lines correspond to $2N(N+1)$ (black) and N (red). (c) Trade-off in the optimality of individual estimations quantified by Υ. In all plots: blue circles, $\epsilon = 0.14$; yellow squares, $\epsilon = 0.23$; green diamonds, $\epsilon = 0.32$; red triangles, $\epsilon = 0.50$; purple inverted triangles, $\epsilon = 1$.

followed by photon-number resolving detectors on each arm. In order to account for distinguishability, we take the standard decomposition $b_V^\dagger = \sqrt{1-\epsilon^2}a_V^\dagger + \epsilon q_V^\dagger$, where $a_V^\dagger$ interferes perfectly with $a_H^\dagger$, while $q_V^\dagger$ does not. The parameter ϵ defines the distinguishability of the two modes: from $\epsilon = 0$ for perfect indistinguishability to $\epsilon = 1$ for complete distinguishability. We are interested in how the available Fisher information associated to ϕ and to ϵ scales with the number of photons N; we use as quantifiers the effective values $\tilde{F}_{i,i} = 1/(F^{-1})_{i,i}$ for $i = \phi, \epsilon$, optimized over all possible phases.

The results of our numerical simulations are reported in Figs. 4(a) and 4(b). For moderate distinguishability, the effective Fisher information on ϕ decreases with respect to its value $2N(N+1)$ at $\epsilon = 0$ [59], but retains a quicker growth than the classical scaling as N, obtained for $\epsilon = 1$. Nevertheless, while the effective Fisher information $\tilde{F}_{\phi\phi}$ is reduced due to the presence of correlation between the two parameters, the plot leads us to conjecture that, as observed in [17] for the phase-estimation-only problem, an asymptotic quadratic scaling is maintained also for distinguishability $0 < \epsilon < 1$. Regarding the distinguishability ϵ, we remark upon a non-monotonic behavior: the information initially decreases with respect to the linear scaling, but a quadratic behavior $2N^2$ is eventually observed in the limit $\epsilon = 1$. Since the phase is the parameter of main interest, even a slow scaling for the uncertainty on the visibility can be tolerated, as long as its estimation remains useful.

The optimal values of $\tilde{F}_{\phi,\phi}$ and $\tilde{F}_{\epsilon,\epsilon}$, however, are obtained for different phases ϕ; in general, it is not possible to satisfy the optimality conditions for both parameters at once. In order to understand how the information is partitioned, we adopt the parameter

$$\Upsilon = \max_{\gamma}\left(\frac{\tilde{F}_{\phi,\phi}(\gamma)}{\max_\alpha \tilde{F}_{\phi,\phi}(\alpha)} + \frac{\tilde{F}_{\epsilon,\epsilon}(\gamma)}{\max_\beta \tilde{F}_{\epsilon,\epsilon}(\beta)}\right). \tag{10}$$

We remark that this figure of merit does not quantify the overall performance of the estimation scheme that, as demonstrated above, generally increases with the number of photons N. Its goal is in turn to study the multi-parameter estimation problem from a more fundamental point of view and to quantify how close one can get to the optimal estimation precision simultaneously for both parameters. To this aim, we calculate the sum of the ratios between the effective Fisher information for ϕ and ϵ, respectively, and their maximum values, optimized for a particular value of ϕ. The corresponding results are show in Fig. 4(c): for each value of ϵ there exists a value of N that achieves the best compromise in the jointly attainable precision. Our numerical results also suggest that, while for highly noisy probes (large values of ϵ) the optimal value occurs for small N, for nearly ideal probes (small values of ϵ), optimality is reached for larger values of N, where the quantum enhancement in the phase estimation is more prominent.

5. CONCLUSIONS

Multiparameter estimation can be an effective way to tackle the problem of operating quantum sensors in the presence of noise, an unavoidable challenge in realistic conditions. We have applied such an approach to integrate phase estimation with a simultaneous characterization of the probe, by measuring phase and visibility of interference fringes at once. Depending on the value of the phase, oscillations in the achieved precision on individual parameters are observed, and correlations are introduced. The measurement scheme has been used to investigate the optical activity of fructose solutions. Numerical simulations have been undertaken to study how the precisions scale with the photon number in Holland–Burnett states.

Our results highlight the presence of trade-off conditions, as part of the information need is devoted to determining the quality of the probe at the expense of the precision on the phase. Realizing the promises of quantum sensing will require understanding the price of achieving robust operation in unfavorable conditions; our study is an important step in this direction.

Funding. FETOPEN-RIA (665148 - QCUMbER); H2020 Marie Skłodowska-Curie Actions (MSCA) (701154).

Acknowledgment. We thank P. Aloe, F. Somma, A. Sodo, F. Bruni, and M. G. A. Paris for useful discussions. M. G. G. acknowledges support from Marie Skłodowska-Curie Action H2020-MSCA-IF-2015 (project ConAQuMe).

See Supplement 1 for supporting content.

REFERENCES

1. V. Giovannetti, S. Lloyd, and L. Maccone, "Quantum-enhanced measurements: beating the standard quantum limit," Science **306**, 1330–1336 (2004).
2. V. Giovannetti, S. Lloyd, and L. Maccone, "Quantum metrology," Phys. Rev. Lett. **96**, 010401 (2006).
3. M. G. A. Paris, "Quantum estimation for quantum technology," Int. J. Quantum Inf. **7**, 125–137 (2009).
4. V. Giovannetti, S. Lloyd, and L. Maccone, "Advances in quantum metrology," Nat. Photonics **5**, 222–229 (2011).

5. R. Demkowicz-Dobrzański, M. Jarzyna, and J. Kolodynski, "Quantum limits in optical interferometry," Prog. Opt. **60**, 345–435 (2015).
6. C. M. Caves, "Quantum-mechanical noise in an interferometer," Phys. Rev. D **23**, 1693–1708 (1981).
7. G. Breitenbach, S. Schiller, and J. Mlynek, "Measurement of the quantum states of squeezed light," Nature **387**, 471–475 (1997).
8. L. A. Rozema, D. H. Mahler, R. Blume-Kohout, and A. M. Steinberg, "Optimizing the choice of spin-squeezed states for detecting and characterizing quantum processes," Phys. Rev. X **4**, 041025 (2014).
9. H. Lee, P. Kok, and J. P. Dowling, "A quantum Rosetta stone for interferometry," J. Mod. Opt. **49**, 2325–2338 (2002).
10. I. Afek, O. Ambar, and Y. Silberberg, "High-noon states by mixing quantum and classical light," Science **328**, 879–881 (2010).
11. J. Joo, W. J. Munro, and T. P. Spiller, "Erratum: quantum metrology with entangled coherent states," Phys. Rev. Lett. **107**, 219902 (2011).
12. U. Dorner, R. Demkowicz-Dobrzanski, B. J. Smith, J. S. Lundeen, W. Wasilewski, K. Banaszek, and I. A. Walmsley, "Optimal quantum phase estimation," Phys. Rev. Lett. **102**, 040403 (2009).
13. M. Kacprowicz, R. Demkowicz-Dobrzański, W. Wasilewski, K. Banaszek, and I. A. Walmsley, "Experimental quantum-enhanced estimation of a lossy phase shift," Nat. Photonics **4**, 357–360 (2010).
14. N. Thomas-Peter, B. J. Smith, A. Datta, L. Zhang, U. Dorner, and I. A. Walmsley, "Real-world quantum sensors: evaluating resources for precision measurement," Phys. Rev. Lett. **107**, 113603 (2011).
15. A. Datta, L. Zhang, N. Thomas-Peter, U. Dorner, B. J. Smith, and I. A. Walmsley, "Quantum metrology with imperfect states and detectors," Phys. Rev. A **83**, 063836 (2011).
16. S. Knysh, V. N. Smelyanskiy, and G. A. Durkin, "Scaling laws for precision in quantum interferometry and the bifurcation landscape of the optimal state," Phys. Rev. A **83**, 021804 (2011).
17. P. M. Birchall, , J. Sabines-Chesterking, J. L. O'Brien, H. Cable, and J. C. F. Matthews, "Beating the shot-noise limit with sources of partially-distinguishable photons," arXiv:1603.00686 (2016).
18. B. M. Escher, R. L. de Matos Filho, and L. Davidovich, "General framework for estimating the ultimate precision limit in noisy quantum-enhanced metrology," Nat. Phys. **7**, 406–411 (2011).
19. R. Demkowicz-Dobrzański, J. Kołodyński, and M. Guţă, "The elusive Heisenberg limit in quantum-enhanced metrology," Nat. Commun. **3**, 1063 (2012).
20. R. Chaves, J. B. Brask, M. Markiewicz, J. Kołodyński, and A. Acín, "Noisy metrology beyond the standard quantum limit," Phys. Rev. Lett. **111**, 120401 (2013).
21. J. B. Brask, R. Chaves, and J. Kołodyński, "Improved quantum magnetometry beyond the standard quantum limit," Phys. Rev. X **5**, 031010 (2015).
22. Y. Matsuzaki, S. C. Benjamin, and J. F. Fitzsimons, "Magnetic field sensing beyond the standard quantum limit under the effect of decoherence," Phys. Rev. A **84**, 012103 (2011).
23. A. W. Chin, S. F. Huelga, and M. B. Plenio, "Quantum metrology in non-Markovian environments," Phys. Rev. Lett. **109**, 233601 (2012).
24. A. Smirne, J. Kołodyński, S. F. Huelga, and R. Demkowicz-Dobrzański, "Ultimate precision limits for noisy frequency estimation," Phys. Rev. Lett. **116**, 120801 (2016).
25. J. F. Haase, A. Smirne, J. Kołodyński, R. Demkowicz-Dobrzański, and S. F. Huelga, "Fundamental limits to frequency estimation: a comprehensive microscopic perspective," New J. Phys. **20**, 053009 (2018).
26. A. Górecka, F. A. Pollock, P. Liuzzo-Scorpo, R. Nichols, G. Adesso, and K. Modi, "Noisy frequency estimation with noisy probes," New J. Phys. (to be published).
27. E. M. Kessler, I. Lovchinsky, A. O. Sushkov, and M. D. Lukin, "Quantum error correction for metrology," Phys. Rev. Lett. **112**, 150802 (2014).
28. G. Arrad, Y. Vinkler, D. Aharonov, and A. Retzker, "Increasing sensing resolution with error correction," Phys. Rev. Lett. **112**, 150801 (2014).
29. W. Dür, M. Skotiniotis, F. Fröwis, and B. Kraus, "Improved quantum metrology using quantum error correction," Phys. Rev. Lett. **112**, 080801 (2014).
30. P. Sekatski, M. Skotiniotis, and W. Dür, "Dynamical decoupling leads to improved scaling in noisy quantum metrology," New J. Phys. **18**, 073034 (2015).
31. M. B. Plenio and S. F. Huelga, "Sensing in the presence of an observed environment," Phys. Rev. A **93**, 032123 (2016).
32. T. Gefen, D. A. Herrera-Martí, and A. Retzker, "Parameter estimation with efficient photodetectors," Phys. Rev. A **93**, 032133 (2016).
33. D. Layden and P. Cappellaro, "Spatial noise filtering through error correction for quantum sensing," npj Quantum Inf. **4**, 30 (2018).
34. P. Sekatski, M. Skotiniotis, J. Kołodyński, and W. Dür, "Quantum metrology with full and fast quantum control," Quantum **1**, 27 (2017).
35. Y. Matsuzaki and S. Benjamin, "Magnetic-field sensing with quantum error detection under the effect of energy relaxation," Phys. Rev. A **95**, 032303 (2017).
36. S. Zhou, M. Zhang, J. Preskill, and L. Jiang, "Achieving the Heisenberg limit in quantum metrology using quantum error correction," Nat. Commun. **9**, 78 (2018).
37. F. Albarelli, M. A. C. Rossi, D. Tamascelli, and M. G. Genoni, "Restoring Heisenberg scaling in noisy quantum metrology by monitoring the environment," arXiv:1803.05891 (2018).
38. A. Orieux, L. Sansoni, M. Persechino, P. Mataloni, M. Rossi, and C. Macchiavello, "Experimental detection of quantum channels," Phys. Rev. Lett. **111**, 220501 (2013).
39. X.-Q. Zhou, H. Cable, R. Whittaker, P. Shadbolt, J. L. O'Brien, and J. C. F. Matthews, "Quantum-enhanced tomography of unitary processes," Optica **2**, 510–516 (2015).
40. R. D. Gill and S. Massar, "State estimation for large ensembles," Phys. Rev. A **61**, 042312 (2000).
41. C. Macchiavello, "Optimal estimation of multiple phases," Phys. Rev. A **67**, 062302 (2003).
42. M. A. Ballester, "Entanglement is not very useful for estimating multiple phases," Phys. Rev. A **70**, 032310 (2004).
43. O. Pinel, P. Jian, N. Treps, C. Fabre, and D. Braun, "Quantum parameter estimation using general single-mode Gaussian states," Phys. Rev. A **88**, 040102 (2013).
44. M. G. Genoni, M. G. A. Paris, G. Adesso, H. Nha, P. L. Knight, and M. S. Kim, "Optimal estimation of joint parameters in phase space," Phys. Rev. A **87**, 012107 (2013).
45. C. Vaneph, T. Tufarelli, and M. Genoni, "Quantum estimation of a two-phase spin rotation," Quantum Meas. Quantum Metrol. **1**, 12-20 (2013).
46. L. Pezzè, M. A. Ciampini, N. Spagnolo, P. C. Humphreys, A. Datta, I. A. Walmsley, M. Barbieri, F. Sciarrino, and A. Smerzi, "Optimal measurements for simultaneous quantum estimation of multiple phases," Phys. Rev. Lett. **119**, 130504 (2017).
47. S. I. Knysh and G. A. Durkin, "Estimation of phase and diffusion: combining quantum statistics and classical noise," arXiv:1307.0470 (2013).
48. P. J. D. Crowley, A. Datta, M. Barbieri, and I. A. Walmsley, "Tradeoff in simultaneous quantum-limited phase and loss estimation in interferometry," Phys. Rev. A **89**, 023845 (2014).
49. M. D. Vidrighin, G. Donati, M. G. Genoni, X.-M. Jin, W. S. Kolthammer, A. D. M. S. Kim, M. Barbieri, and I. A. Walmsley, "Joint estimation of phase and phase diffusion for quantum metrology," Nat. Commun. **5**, 3532 (2014).
50. M. Szczykulska, T. Baumgratz, and A. Datta, "Reaching for the quantum limits in the simultaneous estimation of phase and phase diffusion," Quantum Sci. Technol. **2**, 044004 (2017).
51. E. Roccia, M. G. Genoni, L. Mancino, I. Gianani, M. Barbieri, and M. Sbroscia, "Monitoring dispersive samples with single photons: the role of frequency correlations," Quantum Meas. Quantum Metrol. **4**, 64–69 (2017).
52. C. K. Hong, Z. Y. Ou, and L. Mandel, "Measurement of subpicosecond time intervals between two photons by interference," Phys. Rev. Lett. **59**, 2044–2046 (1987).
53. B. Gendra, E. Ronco-Bonvehi, J. Calsamiglia, R. M. Tapia, and E. Bagan, "Quantum metrology assisted by abstention," Phys. Rev. Lett. **110**, 100501 (2013).
54. J. Combes, C. Ferrie, Z. Jiang, and C. M. Caves, "Quantum limits on post-selected, probabilistic quantum metrology," Phys. Rev. A **89**, 052117 (2014).
55. N. Tischler, M. Krenn, R. Fickler, X. Vidal, A. Zeilinger, and G. Molina-Terriza, "Quantum optical rotatory dispersion," Sci. Adv. **2**, e1601306 (2016).
56. T. Anderson, *An Introduction to Multivariate Statistical Analysis*, 3rd ed. (Wiley, 2003)
57. A. Monras and M. G. A. Paris, "Optimal quantum estimation of loss in bosonic channels," Phys. Rev. Lett. **98**, 160401 (2007).
58. M. G. Genoni, S. Olivares, and M. G. A. Paris, "Optical phase estimation in the presence of phase diffusion," Phys. Rev. Lett. **106**, 153603 (2011).
59. M. J. Holland and K. Burnett, "Interferometric detection of optical phase shifts at the Heisenberg limit," Phys. Rev. Lett. **71**, 1355–1358 (1993).